



OPEN ACCESS

EDITED BY

Vijayakumar Sekar,
Shandong University, China

REVIEWED BY

Partha Roy,
Gandhi Institute of Technology and
Management (GITAM), India
Vishwambhar Bhandare,
Shivaji University, India
Sutapa Mukherjee,
Chittaranjan National Cancer Institute
(CNCI), India

*CORRESPONDENCE

Lamya Ahmed Al-Keridis,
✉ laalkeridis@pnu.edu.sa
Irfan Ahmad Ansari,
✉ ahmadirfan.amu@gmail.com

RECEIVED 27 March 2023

ACCEPTED 22 September 2023

PUBLISHED 17 October 2023

CITATION

Mishra P, Ali Ahmad MF, Al-Keridis LA,
Saeed M, Alshammari N, Alabdallah NM,
Tiwari RK, Ahmad A, Verma M, Fatima S
and Ansari IA (2023), Methotrexate-
conjugated zinc oxide nanoparticles
exert a substantially improved cytotoxic
effect on lung cancer cells by
inducing apoptosis.
Front. Pharmacol. 14:1194578.
doi: 10.3389/fphar.2023.1194578

COPYRIGHT

© 2023 Mishra, Ali Ahmad, Al-Keridis,
Saeed, Alshammari, Alabdallah, Tiwari,
Ahmad, Verma, Fatima and Ansari. This is
an open-access article distributed under
the terms of the [Creative Commons
Attribution License \(CC BY\)](https://creativecommons.org/licenses/by/4.0/). The use,
distribution or reproduction in other
forums is permitted, provided the original
author(s) and the copyright owner(s) are
credited and that the original publication
in this journal is cited, in accordance with
accepted academic practice. No use,
distribution or reproduction is permitted
which does not comply with these terms.

Methotrexate-conjugated zinc oxide nanoparticles exert a substantially improved cytotoxic effect on lung cancer cells by inducing apoptosis

Prakriti Mishra¹, Mohd Faizan Ali Ahmad¹,
Lamya Ahmed Al-Keridis^{2*}, Mohd Saeed³, Nawaf Alshammari³,
Nadiyah M. Alabdallah^{4,5}, Rohit Kumar Tiwari^{1,6}, Afza Ahmad¹,
Mahima Verma¹, Shireen Fatima¹ and Irfan Ahmad Ansari^{1*}

¹Department of Biosciences Integral University Lucknow, Lucknow, India, ²Biology Department, Faculty of Science, Princess Nourah Bint Abdulrahman University, Riyadh, Saudi Arabia, ³Department of Biology, College of Science, University of Hail, Hail, Saudi Arabia, ⁴Department of Biology, College of Science, Imam Abdulrahman Bin Faisal University, Dammam, Saudi Arabia, ⁵Basic and Applied Scientific Research Centre, Imam Abdulrahman Bin Faisal University, Dammam, Saudi Arabia, ⁶Department of Clinical Research, School of Allied Health Sciences, Sharda University, Uttar Pradesh, India

In the current study, we report the synthesis of methotrexate-conjugated zinc oxide nanoparticles (MTX-ZnONPs) and their high efficacy against lung cancer cells. Conjugation of MTX with ZnONPs was authenticated by UV-vis spectroscopy, dynamic light scattering (DLS), Fourier-transform infrared (FTIR) spectroscopy, and transmission electron microscopy (TEM). This drug-nanoconjugate also showed high drug-loading efficiency. The therapeutic efficacy of MTX-ZnONPs was further tested *in vitro* against A549 cells, and the results of MTT and LDH release assays showed that MTX-ZnONPs, in addition to free MTX, were efficient in exerting cytotoxic effect on A549 cells; however, the effectiveness of MTX-ZnONPs was found to be considerably enhanced at very low doses compared to that of free MTX. Moreover, ZnONPs alone significantly inhibited the cell viability of A549 cells at a much higher concentration compared to MTX-ZnONPs and MTX. Furthermore, the cytomorphology of A549 cells was characterized by cellular shrinkage and detachment from the surface in all the treatment groups. Similarly, A549 cells, in all the treatment groups, showed fragmented and condensed nuclei, indicating the initiation of apoptosis. Mitochondrial membrane potential (ψ_m) in A549 cells showed a gradual loss in all the treatment groups. Results of the qualitative and quantitative analyses depicted increased reactive oxygen species (ROS) levels in A549 cells. The results of the caspase activity assay showed that MTX-ZnONPs and free MTX caused significant activation of caspase-9, -8, and -3 in A549 cells; however, the effect of MTX-ZnONPs was more profound at very low doses compared to that of free MTX. Thus, our results showed high efficacy of MTX-ZnONPs, suggesting efficient intracellular delivery of the drug by ZnONPs as nanocarriers.

KEYWORDS

zinc oxide, nanoparticles, methotrexate, lung cancer, A549, reactive oxygen species, caspases

Introduction

Despite recent advancements in molecularly targeted therapy that have fundamentally transformed the therapeutic strategies for lung cancer, chemotherapy is still a key component of lung cancer treatment (Lee, 2019). Whether administered alone or in conjunction with other treatment options, chemotherapy has benefitted patients with early- and late-stage lung cancer in terms of survival and quality of life. Combination therapy with other classes of anticancer agents and new drug delivery systems has shown promising results, and these are currently the focus of ongoing research. The ultimate objective of researchers is to increase therapeutic efficacy and reduce the potential risks associated with a drug.

Methotrexate (MTX) is a well-established drug, widely used in numerous cancer treatments, psoriasis, and rheumatological diseases (Khan et al., 2012). Currently, many forms of cancer, such as osteosarcoma, acute lymphoblastic leukemia, acute myeloid leukemia, meningeal leukemia and lymphoma, non-lymphoma, Hodgkin's lymphoma, breast cancer, and bladder cancer, are treated with MTX in conjunction with other drugs (Frei et al., 1975; Evans et al., 1986; Huennekens, 1994; Crews et al., 2004). MTX is a folic acid analog that inhibits dihydrofolate reductase activity, thereby disrupting cellular folate metabolism (Aghajanzadeh et al., 2018). MTX has been shown to exhibit therapeutic efficacy against numerous types of cancer cells that have overexpress folate receptors on their surface (Duthie, 2001).

The bioavailability of chemotherapeutic drugs, which can cause severe toxicities and off-target side effects, is one of the major challenges in cancer chemotherapy (Gewirtz et al., 2010). One plausible approach to overcome these challenges is the design of a nanocarrier that can selectively deliver cytotoxic doses of therapeutic drugs to cancer cells (Nosrati et al., 2017; Aghajanzadeh et al., 2018; Zamani et al., 2018). Zinc oxide nanoparticles (ZnONPs), one of the nanocarriers used for drug delivery and cancer therapy, have attracted significant interest in drug delivery systems (Barui et al., 2018). ZnONPs are considered as potential candidates for drug delivery due to their easy synthesis from low-cost precursors, biocompatibility, and effective cellular internalization through endocytosis (Duncan and Richardson, 2012; Singh et al., 2020).

When compared to conventional methods, formulation and targeting techniques for MTX using controlled release carriers, multi-articulate approaches, prodrugs, and drug conjugates, have been found to increase bioavailability, minimize adverse effects, and maximize clinical effectiveness (Khan et al., 2012). Previous studies have reported high expression of folate receptors on lung cancer cells (Nunez et al., 2012; O'Shannessy et al., 2012). Moreover, MTX has some affinity for folate receptors because of its structural similarity with folic acid (Xie et al., 2018). Moreover, there is no report to date showing the conjugation of MTX with ZnONPs. Therefore, we hypothesized that due to the high expression of folate receptors on lung cancer cells, MTX-conjugated nanoparticles could potentially be efficiently internalized inside cancer cells and show an increased cytotoxic effect against lung cancer cells. Accordingly, to test this hypothesis, we synthesized and investigated the efficacy of MTX-conjugated

ZnO nanoparticles (MTX-ZnONPs) against an A549 non-small cell lung adenocarcinoma cell line.

Materials and methods

Materials

Methotrexate, 1-ethyl-3-(3-dimethyl) carbodiimide (EDC), 2',7'-dichlorodihydrofluorescein diacetate (H₂DCFDA), 4',6-diamidino-2-phenylindole (DAPI), 3-(4,5-dimethylthiazol-2-yl)-2,5-diphenyltetrazolium bromide (MTT), and Rhodamine 123 were purchased from Sigma-Aldrich (St. Louis, United States). Dulbecco's Modified Eagle Medium, antibiotic-antimycotic solution (penicillin, streptomycin, and amphotericin B), fetal bovine serum (FBS), and LDH Cytotoxicity Assay Kit were procured from Gibco (Thermo Fisher Scientific, Waltham, United States). Caspase-9, -8, and -3 assay kits were procured from BioVision (Milpitas, United States). All other chemicals were of analytical grade.

Methods

Biosynthesis and characterization of ZnONPs

The synthesis process of the fungus (*Aspergillus niger* OL636020)-mediated ZnONPs and their characterization by FTIR, DLS, zeta potential, TEM, and UV-vis spectroscopy analysis were discussed in our previous publication [13].

Conjugation of MTX with ZnONPs

MTX was conjugated with biogenically synthesized ZnONPs. The conjugation was achieved using an EDC coupler, which reacts with carboxyl groups present on ZnONPs and the amino group of MTX to produce MTX-ZnONPs. Briefly, 1 mL of the reaction mixture was prepared by adding 50 mM HEPES buffer, MTX (3 mg/mL), 800 μ L of ZnONP suspension, and 5 mM EDC. The mixture was incubated for 5 h at 30°C. Finally, MTX-ZnONPs were separated via centrifugation at 10,000 rpm for 10 min.

Drug loading efficiency of ZnONPs

The loading percentage of MTX on ZnONPs was determined by measuring the absorbance before and after conjugation at 302 nm. The loading efficiency of the nanoparticle was calculated using the following formula:

$$\text{Percent Loading of MTX on ZnONPs} = [(A - B) \times \frac{100}{A}],$$

where A represents the absorbance of the whole drug added to ZnONPs and B represents the absorbance of the unbound drug in the supernatant of the drug-nanoparticle conjugate solution.

Characterization of MTX-conjugated ZnONPs

MTX-ZnONPs were characterized by UV-vis spectrophotometry (Shimadzu dual-beam spectrophotometer, model UV-1601 PC, 1 nm

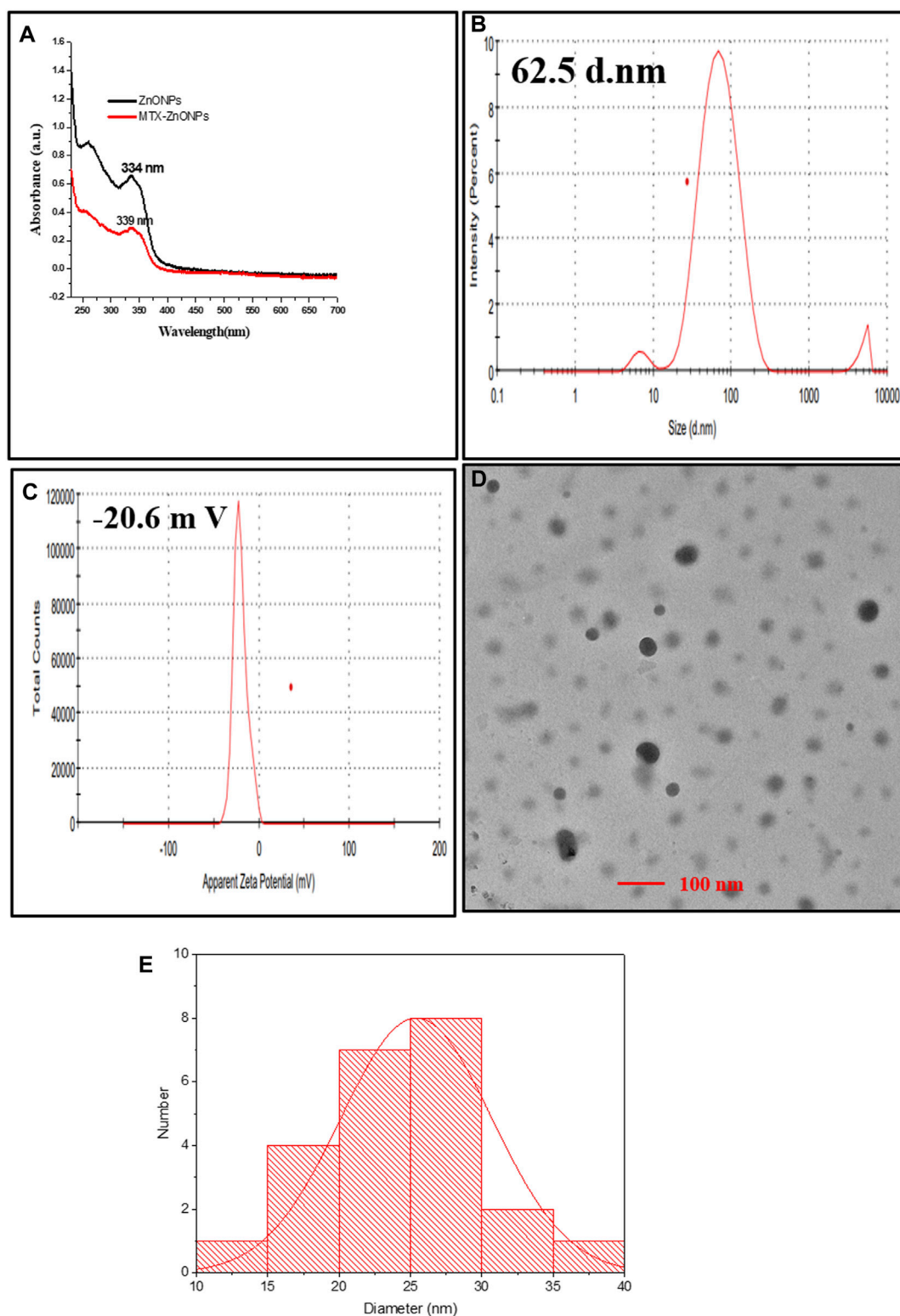


FIGURE 1

Characterization of MTX-ZnONPs under (A) UV-visible spectra (339 nm), (B) hydrodynamic diameter (62.5 nm), (C) zeta potential (-20.6 mV), and (D) transmission electron microscopy (size 25.4 nm). (E) Size distribution graph showing the size of MTX-ZnONPs (25.407 ± 5.295 nm).

resolution. Kyoto, Japan). The mean particle size and zeta potential of MTX-ZnONPs were determined using a particle size analyzer (Zetasizer Nano-ZS, Model ZEN3600, Malvern Instruments Ltd., Malvern,

United Kingdom) [(Gomathy and Sabarinathan, 2010), 15]. Transmission electron microscope (Tecnai™ G2 Spirit Bio-TWIN, FEI, Hillsboro, United States) was used to investigate the size of the

inorganic core at an accelerating voltage of 80 kV (Khan S. et al., 2018). The binding confirmation of MTX on the surface of ZnONPs was analyzed by Fourier-transform infrared spectroscopy (FTIR) (Shimadzu FTIR-8201 PC infrared spectrophotometer) operating in the diffuse reflectance mode at a resolution of 4 cm⁻¹. A total of 256 scans of the ZnONPs film (400–4,000 cm⁻¹ range) were acquired to obtain good signal-to-noise ratios.

Cell culture

A549 cells were purchased from the National Centre for Cell Science (NCCS), Pune, India. The cells were cultured in DMEM, supplemented with 10% FBS and 1% antibiotic-antimycotic solution, in a humidified atmosphere containing 5% CO₂ at 37°C.

Assessment of cytotoxicity

To assess the cytotoxic effect of MTX-ZnONPs and MTX and ZnONPs alone, A549 cells (5 × 10³ per well) were treated with various doses of MTX-ZnONPs and MTX and ZnONPs alone, for 24 h. Then, 10 μL of MTT dye (5 mg/mL in PBS) was added to each well, followed by incubation for 2 h. Later, 100 μL DMSO was added to each well to solubilize the formazan crystals formed by viable cells. Finally, the absorbance of each well was measured at 570 nm using a microplate reader (Bio-Rad, United States). The results were expressed as percent cell viability, which was calculated using the following formula:

$$\text{Cell viability (\%)} = \frac{\text{Average of } A_t}{\text{Average of } A_c} \times 100,$$

where A_t and A_c are the absorbances of the treated and untreated control wells, respectively.

LDH cytotoxicity assay

Briefly, A549 cells (5 × 10³ per well) were placed in a 96-well plate, then co-cultured with various doses of MTX-ZnONPs and MTX and ZnONPs alone for 24 h. Subsequently, LDH activity was measured in all the treatment groups, as per the manufacturer's instructions. Then, the percent cytotoxicity in A549 cells in all the treatment groups, was calculated using the following formula:

$$\% \text{ Cytotoxicity} = \frac{(\text{Drug Treated LDH activity}) - (\text{Spontaneous LDH activity})}{\text{Maximum LDH activity} - \text{Spontaneous LDH activity}} \times 100.$$

Examination of the morphological alterations

Briefly, A549 cells (5 × 10³ per well) were co-cultured with isoeffective doses (IC₂₅, IC₅₀, and IC₇₅) of MTX-ZnONPs, MTX alone, and ZnONPs alone for 24 h. Subsequently, the changes in cellular morphology of cells in all the treatment groups were examined, and images were taken using the relief phase channel of the FLoid imaging station (ThermoScientific, United States).

Assessment of nuclear changes

Nuclear changes in A549 cells were assessed by staining with DAPI dye. The cells (1 × 10⁴ per well) were treated with isoeffective doses of MTX-ZnONPs, MTX alone, and ZnONPs alone for 24 h, followed by washing with PBS and fixing in 4% paraformaldehyde for 10 min. Cells were permeabilized with permeabilizing buffer (0.25% Triton X-100) and, subsequently, stained with DAPI dye (300 nM). Finally, the cells were observed under a blue filter using the FLoid imaging station (ThermoScientific, United States).

Analysis of mitochondrial membrane potential ($\Delta\Psi_m$)

Mitochondrial membrane potential in lung cancer cells was examined via Rhodamine 123 staining. Briefly, A549 cells (1 × 10⁵ cells per well) were grown in a 24-well plate, followed by treatment with isoeffective concentrations of MTX-ZnONPs and MTX and ZnONPs alone for 24 h. Later, the cells were washed and stained with Rhodamine 123 (300 nM) for 30 min in the dark, and photomicrographs were taken using a FLoid imaging station (ThermoScientific, United States).

Detection and quantification of cytosolic reactive oxygen species (ROS)

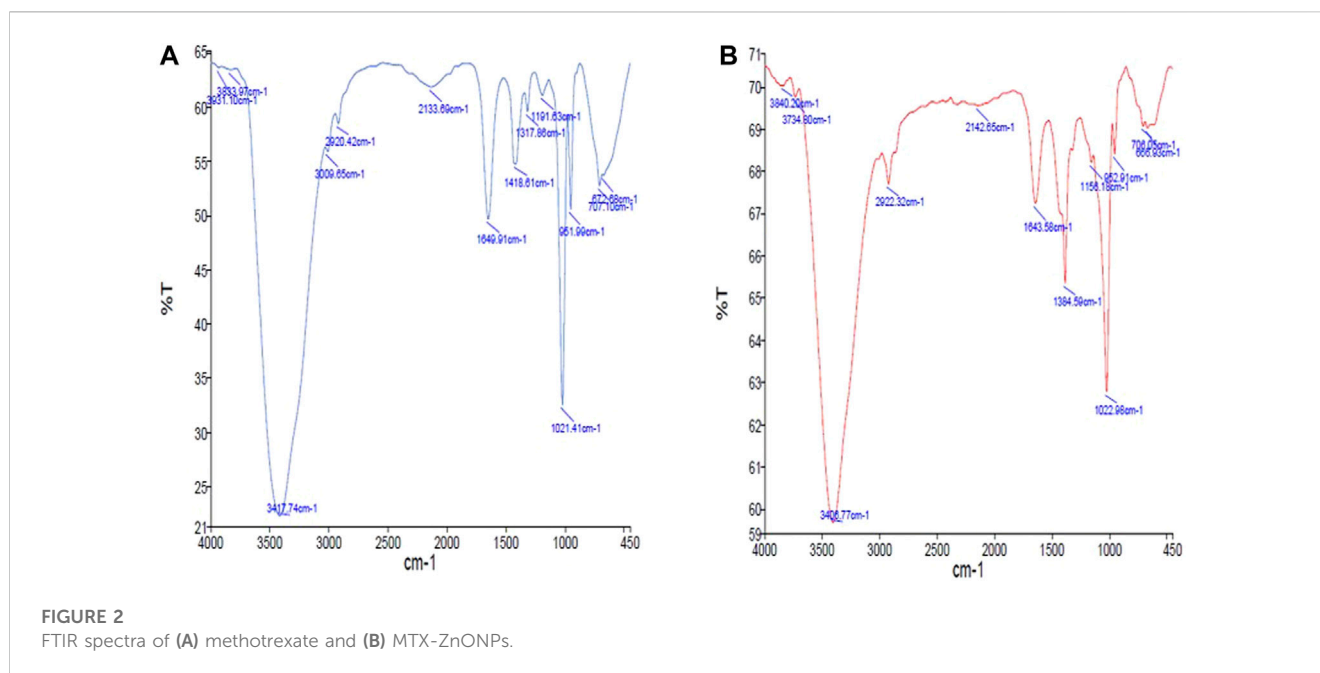
The cytosolic ROS in A549 cells was detected by a fluorogenic dye (H₂DCFDA). Briefly, A549 cells (5 × 10⁴ per well) were treated with isoeffective doses of MTX-ZnONPs as well as MTX and ZnONPs alone for 6 h. Thereafter, the cells were stained with H₂DCFDA (25 μM) for 30 min at 37°C, followed by washing of excess dye with phosphate-buffered saline (PBS). Finally, photomicrographs were captured using the green fluorescence channel of a FLoid imaging station (Thermo Scientific, United States).

For the quantification of cytosolic ROS, A549 cells (1 × 10⁴ per well) in a 96-well black-bottomed culture plate were treated with various doses of MTX-ZnONPs, MTX alone, and ZnONPs alone for 6 h, followed by incubation with H₂DCFDA (25 μM) for 30 min at 37°C. Fluorescence intensity was measured using a multi-well microplate reader (Synergy H1 hybrid multi-mode microplate reader, BioTek, United States). Values were shown as percent DCF fluorescence relative to the untreated control.

To further confirm the role of ROS in drug-nanoparticle conjugate-induced apoptosis, A549 cells were pretreated with 5 mM NAC for 2 h, followed by various doses of MTX-ZnONPs, MTX alone, and ZnONPs alone for another 24 h. Thereafter, cell viability was determined in each treatment group by MTT assay.

Measurement of caspase activity

The activation of caspases in A549 cells was determined using caspase-9, -8, and -3 assay kits to find out the mode of apoptosis in lung cancer cells. Briefly, A549 cells (1 × 10⁶) were co-cultured with various doses of MTX-ZnONPs, MTX alone, and ZnONPs alone for 24 h. Later, caspase activity was measured as per the manufacturer's protocol.



Evaluation of the effect of caspase inhibitors

Caspase-3 inhibitor was used to confirm the activation of caspases and ultimately program cell death in lung cancer cells due to drug–nanoparticle conjugate treatment. Briefly, A549 cells were pretreated with 50 μ M of each caspase inhibitor for 2 h, followed by treatment with various doses of MTX-ZnONPs, MTX alone, and ZnONPs alone for another 24 h. Finally, cell survival in each treatment group was evaluated using the MTT assay.

Statistical analysis

The data are represented as the mean \pm SEM of three separate experiments that were carried out in triplicate. One-way ANOVA with Dunnett's *post hoc* test, two-way ANOVA with Bonferroni's *post hoc* test, and paired *t*-test (GraphPad Prism 8.0) were used to determine significance in various treatment groups ($*p < 0.05$, $**p < 0.01$, and $***p < 0.001$ denote significant differences between means of various treatment groups).

Results

Characterization of drug–nanoparticle conjugates

Conjugation of MTX with ZnONPs was characterized by observing the spectra of drug–nanoparticle conjugate solution, which depicted a shift of the characteristic wavelength of ZnONPs (334 nm to 339 nm) (Figure 1A). Furthermore, the hydrodynamic diameter of drug–nanoparticle conjugates was found to be 62.5 nm, which was higher than that of ZnONPs (53.28 nm) (Figure 1B). The zeta potential of MTX-ZnONPs was observed to be -20.6 mV, slightly higher than that of ZnONPs (-21.4 mV), which describes the good

stability of drug–nanoconjugate (Figure 1C). The average size and shape of the MTX-ZnONPs were further validated by TEM. The average size of drug–nanoparticle conjugates, as shown in the size distribution graph, was 25.4 nm, which was greater than that of ZnONPs (17.2 nm) (Figures 1D,E). Moreover, the shape of drug–nanoconjugates was spherical, and they were found to be monodispersed.

The FTIR spectrum of ZnONPs was shown in our previously published article [13]. In the FTIR spectrum of MTX, the bend peaks of $-\text{OH}$, $-\text{NH}_2$, and $-\text{COOH}$ groups were observed at $3,417$ cm^{-1} , $1,649$ cm^{-1} , and $2,133$ cm^{-1} , respectively (Figure 2B). The stretch peak of the aromatic ring was observed at $2,920$ cm^{-1} . The FTIR spectrum of the prepared MTX-ZnONPs exhibited strong absorption bands at $3,406$ cm^{-1} , corresponding to the $-\text{OH}$ group stretching (Figure 2C). A new peak was observed at $1,643$ cm^{-1} , corresponding to the bend peak of the N-H bond. A new peak was also observed at $1,022$ cm^{-1} , corresponding to the stretch of C-N of the peptide bond, which confirmed the conjugation. Interestingly, in the spectrum of MTX-ZnONPs, the stretch peak of the aromatic ring of MTX was observed at $2,922$ cm^{-1} . The presence of these peaks in MTX-ZnONPs confirmed the conjugation of MTX with ZnONPs.

Percent drug loading

The amount of MTX conjugated with ZnONPs was shown as percent drug loading or drug loading efficiency, which was found to be $82.04\% \pm 3.78\%$. Thus, the result showed high conjugation of MTX with ZnONPs.

Cytotoxicity assay

As shown in Figure 4.3, MTX-ZnONPs (100–800 ng/mL) significantly reduced the viability of A549 cells after 24 h of

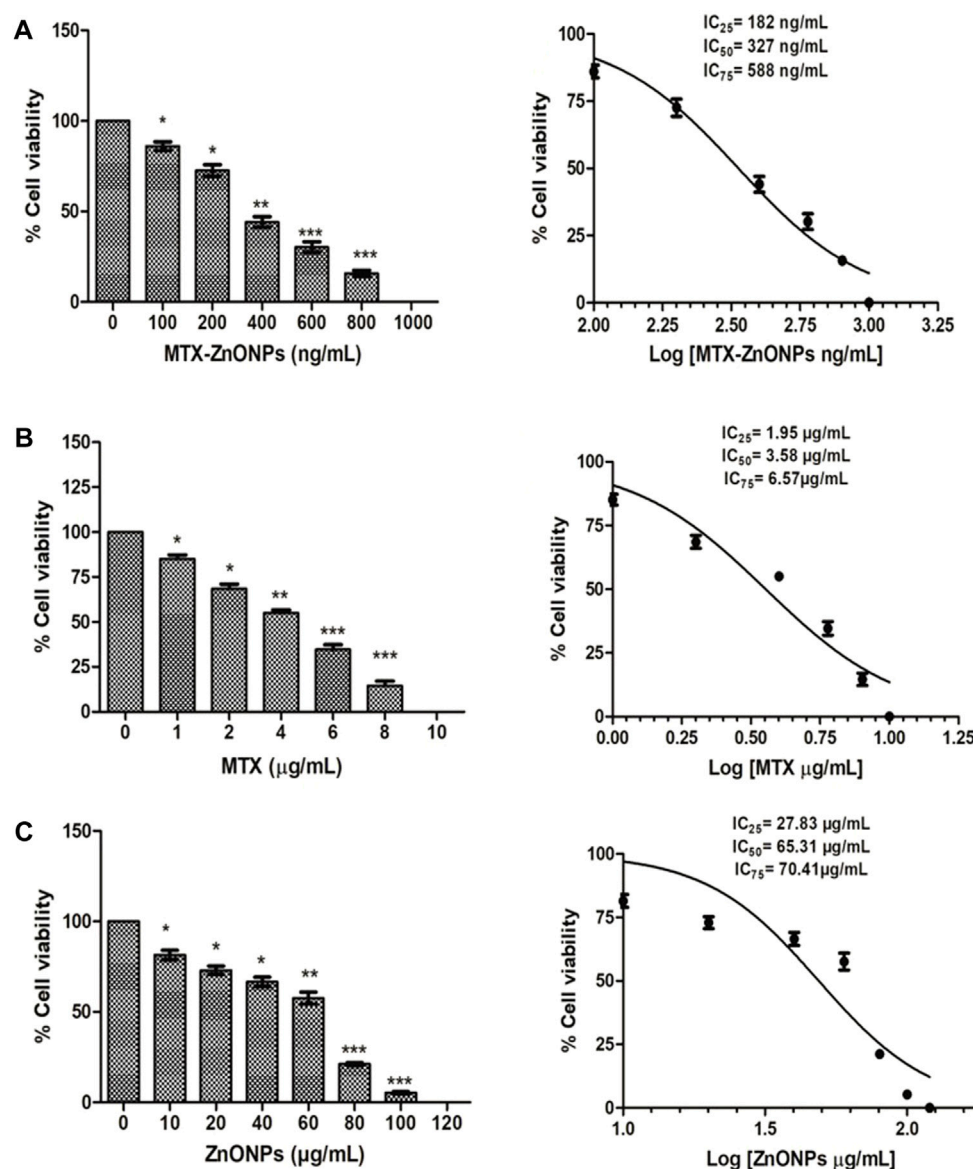


FIGURE 3

Percent cell viability of A549 cells treated with (A) MTX-ZnONPs, (B) MTX alone, and (C) ZnONPs alone for 24 h assessed by MTT assay. The results presented are the mean \pm SEM of three independent experiments performed in triplicate. Significance among different dosage groups were determined using one-way ANOVA followed by Dunnett's *post hoc* test (where * p < 0.05, ** p < 0.01, and *** p < 0.001 represent significant differences compared with vehicle control).

treatment. The cell viability was found to be $86.07\% \pm 2.37\%$, $72.6\% \pm 3.20\%$, $44.10\% \pm 2.94\%$, $30.20\% \pm 2.93\%$, and $15.69\% \pm 1.69\%$ at the doses of 100, 200, 400, 600, and 800 ng/mL MTX-ZnONPs, respectively (Figure 3A). Similarly, MTX alone also significantly inhibited the survival of A549 cells, and the viability was found to be $85.14\% \pm 2.12\%$, $68.57\% \pm 2.54\%$, $55.03\% \pm 1.61\%$, $34.63\% \pm 2.65\%$, and $14.59\% \pm 2.42\%$ at the doses of 1, 2, 4, 6, and 8 $\mu\text{g/mL}$ MTX, respectively (Figure 3B). However, cytotoxic doses of ZnONPs alone for A549 cells were found to be in the range of 10–100 $\mu\text{g/mL}$, and the cell viability was found to be $81.48\% \pm 2.53\%$, $72.97\% \pm 2.31\%$, $66.54\% \pm 2.62\%$, $57.62\% \pm 3.32\%$, $21.18\% \pm 0.79\%$, and 5.32 ± 0.55 at the doses of 10, 20, 40, 60, 80, and 100 $\mu\text{g/mL}$ ZnONPs, respectively (Figure 3C). Furthermore, we also performed the cytotoxicity assay of

ZnONPs against normal 3T3 cells and found that ZnONPs also significantly inhibited the growth of 3T3 cells at a dose of 10–100 $\mu\text{g/mL}$ (Supplementary Figure S1).

The isoeffective concentrations (IC_{25} , IC_{50} , and IC_{75}) of MTX-ZnONPs were found to be 182 ng/mL, 327 ng/mL, and 588 ng/mL, respectively. Similarly, the IC_{25} , IC_{50} , and IC_{75} of MTX alone were 1.95 $\mu\text{g/mL}$, 3.58 $\mu\text{g/mL}$, and 6.57 $\mu\text{g/mL}$, respectively. However, the IC_{25} , IC_{50} , and IC_{75} of ZnONPs alone were 27.83 $\mu\text{g/mL}$, 65.30 $\mu\text{g/mL}$, and 70.41 $\mu\text{g/mL}$, respectively. According to the aforementioned data, the IC_{25} of MTX-ZnONPs was found to be reduced by approximately 10.71-fold, while the IC_{50} was reduced by approximately 10.95-fold compared to MTX alone. Thus, the isoeffective concentrations of MTX-ZnONPs were significantly

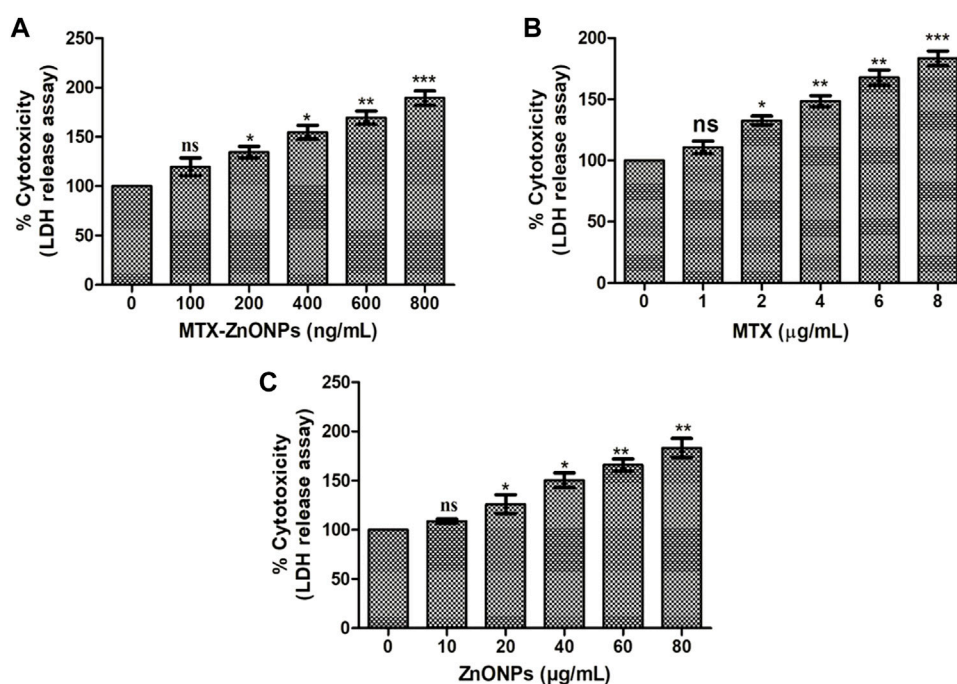


FIGURE 4

Percent cytotoxicity of A549 cells treated with different doses of (A) MTX-ZnONPs, (B) MTX alone, and (C) ZnONPs alone for 24 h assessed by LDH release assay. The results presented are the mean \pm SEM of three independent experiments performed in triplicate. Significance among different dosage groups were determined using one-way ANOVA followed by Dunnett's *post hoc* test (where * $p < 0.05$, ** $p < 0.01$, and *** $p < 0.001$ represent significant differences compared with vehicle control).

reduced compared to MTX alone, which substantiated that MTX-ZnONPs exhibited a similar effect on A549 non-small cell lung cancer cells at a much lower concentration compared to MTX. The results also emphasized the efficient delivery of drug-conjugated ZnONPs.

LDH release assay

The result of the LDH assay revealed that treatment of A549 cells with MTX-ZnONPs for 24 h resulted in a significant amount of cell death, and the percent cytotoxicity was found to be $19.52\% \pm 5.22\%$, $34.45\% \pm 3.37\%$, $54.78\% \pm 4.02\%$, $69.44\% \pm 3.84\%$, and $89.40\% \pm 4.14\%$ at the doses of 100, 200, 400, 600, and 800 ng/mL, respectively (Figure 4A). Similarly, MTX alone also caused significant cell death in A549 cells, and the percent cytotoxicity was found to be $10.65\% \pm 2.96\%$, $32.58\% \pm 2.12\%$, $48.45\% \pm 2.60\%$, $67.77\% \pm 3.53\%$, and $83.40\% \pm 3.47\%$ at the doses of 1, 2, 4, 6, and 8 $\mu\text{g/mL}$, respectively (Figure 4B). Furthermore, ZnONPs alone exerted a cytotoxic effect on A549 cells only at a dose of 10–80 $\mu\text{g/mL}$ (Figure 4C). Thus, the aforementioned results further established that, at similar doses, drug-nanoconjugate treatment led to a greater amount of death in A549 cells compared to drug alone treatment. This assay also indicated the effective intracellular delivery of the drug via zinc oxide nanocarriers.

Morphological alterations

To analyze morphological alterations in lung cancer cells, A549 cells were treated with isoeffective doses of MTX-ZnONPs,

and MTX and ZnONPs alone. The morphology of A549 cells was significantly altered in all the treated groups after 24 h of treatment with IC_{25} (MTX-ZnONPs 182 ng/mL; MTX 1.95 $\mu\text{g/mL}$; and ZnONPs 27.83 $\mu\text{g/mL}$), IC_{50} (MTX-ZnONPs 327 ng/mL; MTX 3.58 $\mu\text{g/mL}$; and ZnONPs 65.3 $\mu\text{g/mL}$), and IC_{75} (MTX-ZnONPs 588 ng/mL; MTX 6.57 $\mu\text{g/mL}$; and ZnONPs 70.41 $\mu\text{g/mL}$) concentrations. A well-spread flattened morphology of cells was observed in the untreated control group, while a round morphology with cell shrinkage was observed in all the treatment groups. Membrane blebbing and lysis were also observed in some proportion of cells among all the treated groups, suggesting their cytotoxicity at the respective doses (Figure 5). As the treatment doses were increased from IC_{25} to IC_{75} , the morphological alterations in A549 cells gradually increased in all the treated groups. As observed previously, MTX-ZnONPs induced similar changes in the cytomorphology of A549 cells at much lower doses compared with MTX, which also indicated the effective delivery of the drug by the carrier nanoparticles.

Nuclear alterations

After treatment with IC_{25} , IC_{50} , and IC_{75} of MTX-ZnONPs, MTX alone, and ZnONPs alone for 24 h, substantial nuclear condensation and fragmentation in A549 cells were observed in all the treatment groups, whereas normal nuclear morphology was observed in the untreated control group (Figure 6). As the treatment doses were increased from IC_{25} to IC_{75} , the nuclear alterations in A549 cells gradually increased in all the treatment groups. The result showed that MTX-ZnONPs exhibited corresponding nuclear

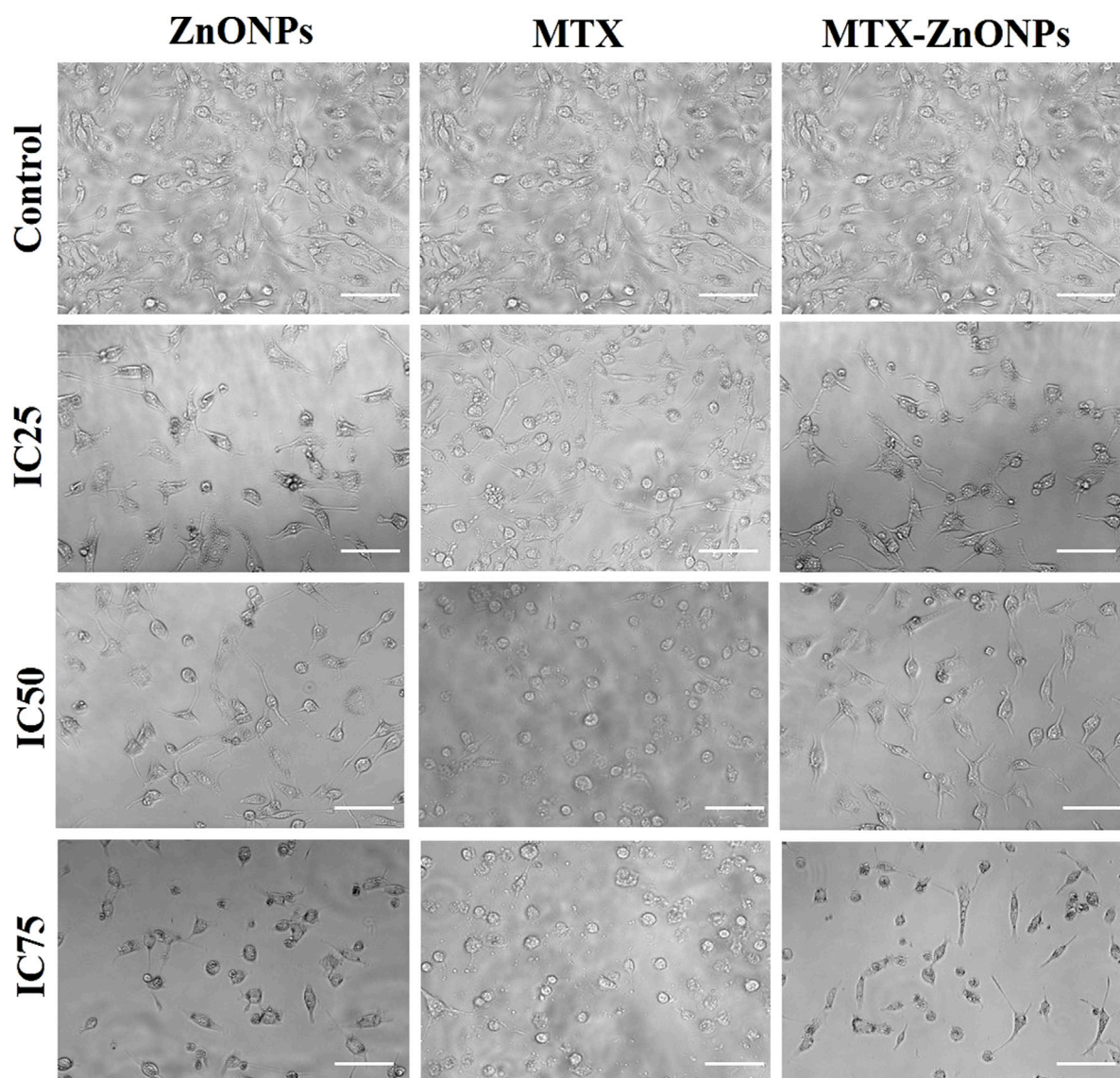


FIGURE 5

Cytomorphological images of A549 cells treated with IC₂₅ (ZnONPs 27.83 $\mu\text{g}/\text{mL}$; MTX 1.95 $\mu\text{g}/\text{mL}$; and MTX-ZnONPs 182 ng/mL), IC₅₀ (ZnONPs 65.30 $\mu\text{g}/\text{mL}$; MTX 3.58 $\mu\text{g}/\text{mL}$; and MTX-ZnONPs 327 ng/mL), and IC₇₅ (ZnONPs 70.41 $\mu\text{g}/\text{mL}$; MTX 6.57 $\mu\text{g}/\text{mL}$; and MTX-ZnONPs 588 ng/mL) concentrations for 24 h analyzed by phase contrast microscopy. Images shown are representative of three independent experiments performed in triplicate (magnification $\times 20$; scale bar 100 μm). The control image was reused in each treatment group.

changes in A549 cells at much lower concentrations compared to MTX. Furthermore, the nuclear condensation in A549 cells suggested the initiation of apoptosis induced by the drug.

Disrupted mitochondrial membrane potential ($\Delta\Psi\text{m}$)

After treatment with IC₂₅, IC₅₀, and IC₇₅ of MTX-ZnONPs, MTX alone, and ZnONPs alone for 24 h, A549 cells exhibited a significant loss of $\Delta\Psi\text{m}$ in all the treatment groups (Figure 7). The fluorescence intensity of Rhodamine 123 in A549 cells, in all the treatment groups, was proportional to $\Delta\Psi\text{m}$. Maximum fluorescence intensity was observed in the untreated control group, while reduced

fluorescence was observed in all the treatment groups. As the treatment doses were increased from IC₂₅ to IC₇₅, the Rhodamine 123 fluorescence in A549 cells gradually decreased in all the treatment groups. Our result demonstrated that MTX-ZnONPs caused an equivalent reduction in $\Delta\Psi\text{m}$ in A549 cells at much reduced concentrations compared with MTX. Moreover, the loss of $\Delta\Psi\text{m}$ in A549 cells indicated the initiation of the intrinsic pathway of apoptosis caused by the aforementioned drug.

Augmented ROS production

The intracellular ROS level was found to be enhanced in A549 cells treated with IC₂₅, IC₅₀, and IC₇₅ of MTX-ZnONPs,

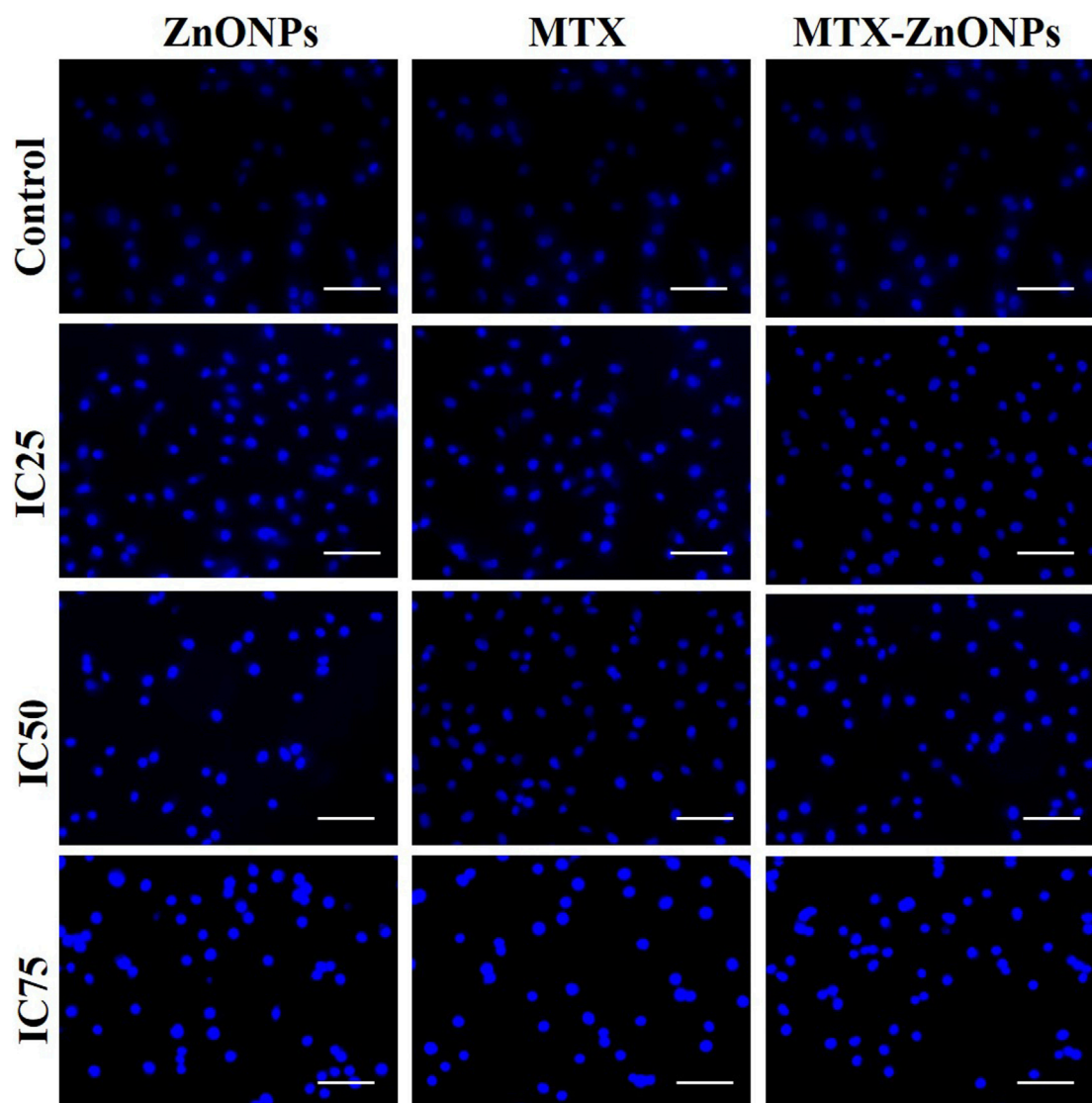


FIGURE 6

Nuclear morphology of DAPI-stained nuclei of A549 cells treated at IC_{25} (ZnONPs 27.83 $\mu\text{g}/\text{mL}$; MTX 1.95 $\mu\text{g}/\text{mL}$; and MTX-ZnONPs 182 ng/mL), IC_{50} (ZnONPs 65.30 $\mu\text{g}/\text{mL}$; MTX 3.58 $\mu\text{g}/\text{mL}$; and MTX-ZnONPs 327 ng/mL), and IC_{75} (ZnONPs 70.41 $\mu\text{g}/\text{mL}$; MTX 6.57 $\mu\text{g}/\text{mL}$; and MTX-ZnONPs 588 ng/mL) concentrations for 24 h analyzed by fluorescence microscopy. Images shown are representative of three independent experiments (scale bar: 100 μm ; magnification: $\times 20$). The control image was reused in each treatment group.

MTX alone, and ZnONPs alone for 24 h (Figure 8). The DCF fluorescence intensity in A549 cells was proportional to the level of ROS in all the treatment groups. The untreated control cells demonstrated insignificant fluorescence, while augmented fluorescence was observed in all the treatment groups. As the treatment doses were increased from IC_{25} to IC_{75} , the intracellular ROS level in A549 cells gradually increased in all the treatment groups. The result showed that MTX-ZnONPs caused a similar increment in cellular ROS production in A549 cells at much lower concentrations compared to MTX. Moreover, the enhanced ROS production in A549 cells indicated the activation of the apoptotic pathway induced by the drug.

In an additional experiment, we also quantified the amount of ROS produced in lung cancer cells treated with MTX-ZnONPs and

MTX and ZnONPs alone. The result demonstrated a dose-dependent increase of DCF fluorescence in A549 cells treated with MTX-ZnONPs, which was found to be $13.38\% \pm 2.96\%$, $28.29\% \pm 3.47\%$, $50.35\% \pm 4.68\%$, $64.84\% \pm 4.06\%$, and $82.62\% \pm 4.12\%$ at the doses of 100, 200, 400, 600, and 800 ng/mL, respectively (Figure 9A). Similarly, MTX alone also caused a significant augmentation of DCF fluorescence in A549 cells, which was found to be $13.47\% \pm 3.49\%$, $33.34\% \pm 3.39\%$, $52.78\% \pm 3.49\%$, $71.21\% \pm 3.74\%$, and $80.17\% \pm 3.87\%$ at the doses of 1, 2, 4, 6, and 8 $\mu\text{g}/\text{mL}$, respectively (Figure 9B). Furthermore, ZnONPs alone exhibited significant DCF fluorescence in A549 cells at a dose of 10–80 $\mu\text{g}/\text{mL}$ (Figure 9C). Our result demonstrated that, at similar doses, MTX-ZnONP treatment led to the generation of a greater

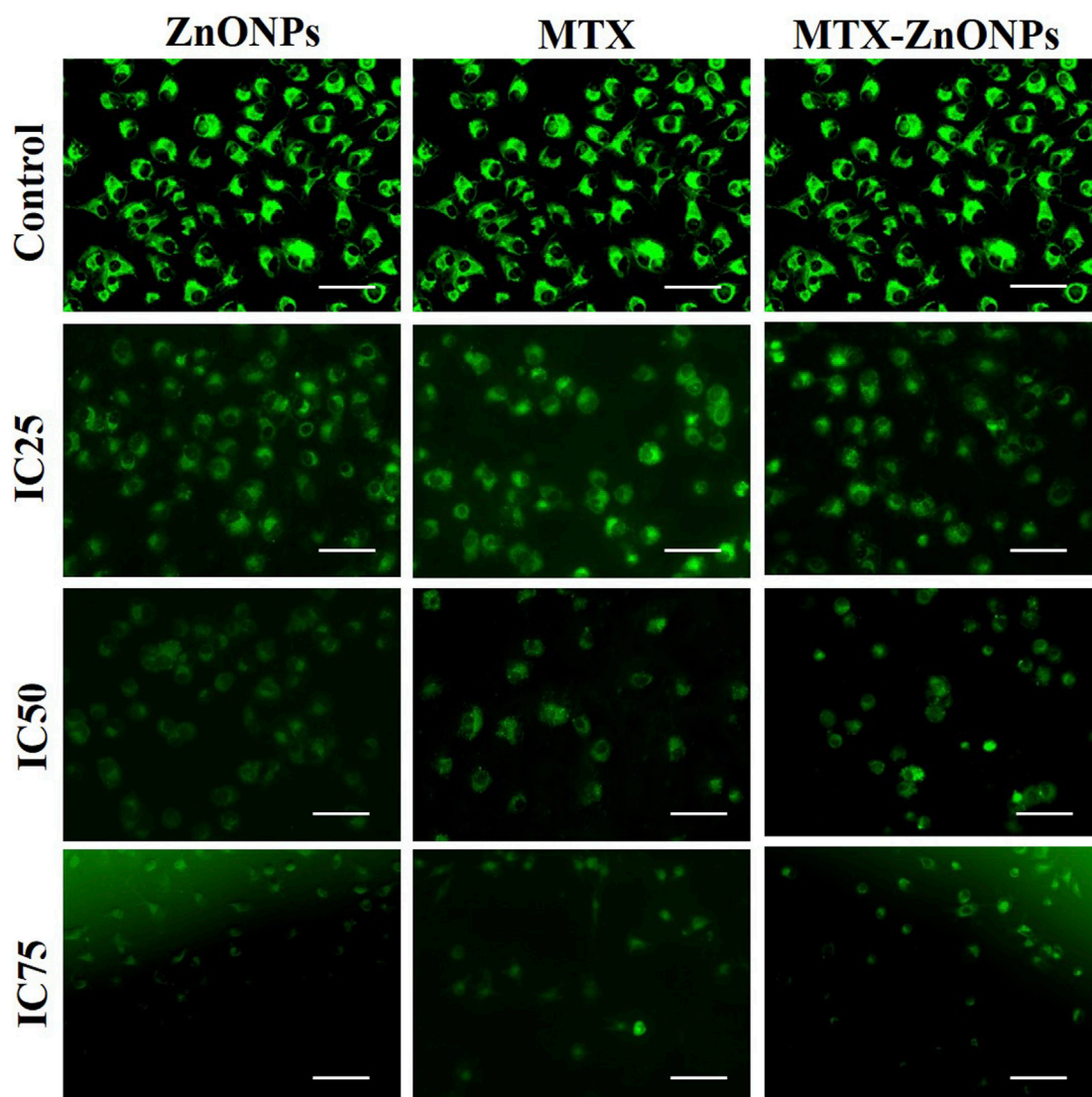


FIGURE 7

Qualitative assessment of mitochondrial membrane potential in Rhodamine 123-stained A549 cells treated at IC₂₅ (ZnONPs 27.83 $\mu\text{g}/\text{mL}$; MTX 1.95 $\mu\text{g}/\text{mL}$; and MTX-ZnONPs 182 ng/mL), IC₅₀ (ZnONPs 65.30 $\mu\text{g}/\text{mL}$; MTX 3.58 $\mu\text{g}/\text{mL}$; and MTX-ZnONPs 327 ng/mL), and IC₇₅ (ZnONPs 70.41 $\mu\text{g}/\text{mL}$; MTX 6.57 $\mu\text{g}/\text{mL}$; and MTX-ZnONPs 588 ng/mL) concentrations for 24 h analyzed by fluorescence microscopy. Images shown are representative of three independent experiments (scale bar: 100 μm ; magnification: $\times 20$). The control image was reused in each treatment group.

amount of ROS in A549 cells compared to treatment with MTX alone.

NAC reduced cytotoxicity

Pretreatment of NAC considerably reduced the cytotoxicity in A549 cells caused by MTX-ZnONPs, MTX alone, and ZnONPs alone (Figure 10). Our findings authenticated the fact that an enhanced level of ROS in all the treatment groups was critical for apoptosis in A549 cells. However, it was interesting to note that the cytotoxicity of MTX-ZnONPs, and MTX and ZnONPs alone, was not completely abrogated by NAC, which implicated the involvement of some ROS-independent apoptotic pathways in all the treatment groups.

Activation of caspases

To determine whether apoptosis in lung cancer cells was due to the activation of caspase-dependent or caspase-independent pathways, caspase activities were determined in A549 cells treated with the effective doses of MTX-ZnONPs and MTX and ZnONPs alone. The caspase-9 activity in the MTX-ZnONP-treated group was substantially augmented by 15.17% \pm 2.01%, 32.70% \pm 4.05%, 56.94% \pm 4.33%, 73.50% \pm 3.14%, and 91.54% \pm 1.86% compared to the untreated control at the doses of 100, 200, 400, 600, and 800 ng/mL, respectively (Figure 11A). Similarly, MTX alone also exhibited significantly increased caspase-9 activity in A549 cells by 10.94% \pm 2.81%, 20.03% \pm 4.06%, 39.61% \pm 4.14%, 64.17% \pm 3.28%, and 87.87% \pm 3.42% at the doses of 1, 2, 4, 6, and 8 $\mu\text{g}/\text{mL}$, respectively (Figure 11B). Furthermore, the activity of caspase-3

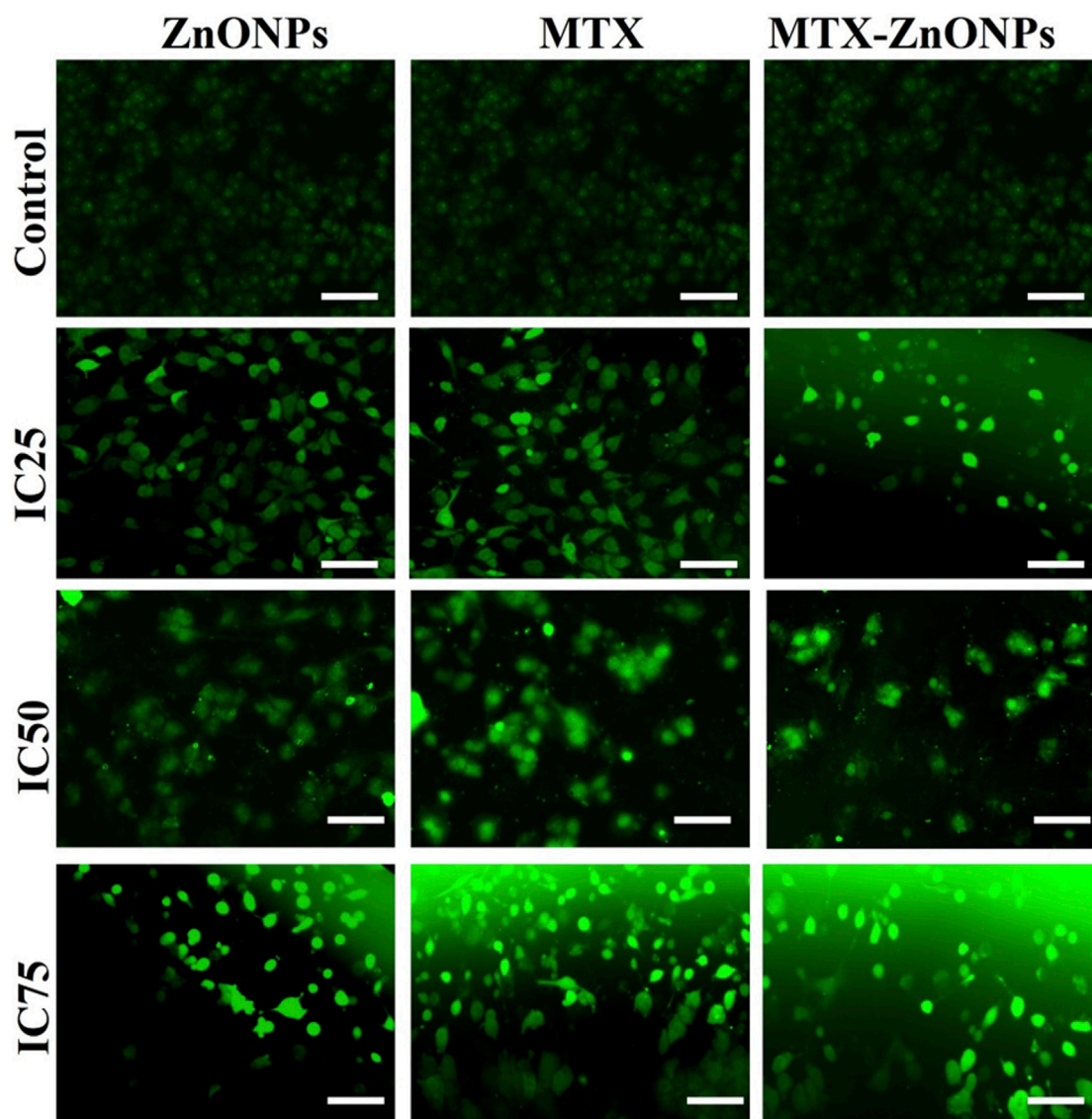


FIGURE 8

Qualitative evaluation of ROS in H₂DCFDA-stained A549 cells treated at IC₂₅ (ZnONPs 27.83 μg/mL; MTX 1.95 μg/mL; and MTX-ZnONPs 182 ng/mL), IC₅₀ (ZnONPs 65.30 μg/mL; MTX 3.58 μg/mL; and MTX-ZnONPs 327 ng/mL), and IC₇₅ (ZnONPs 70.41 μg/mL; MTX 6.57 μg/mL; and MTX-ZnONPs 588 ng/mL) concentrations for 24 h analyzed by fluorescence microscopy. Images shown are representative of three independent experiments (scale bar: 100 μm; magnification: ×20). The control image was reused in each treatment group.

was significantly enhanced in MTX-ZnONP-treated A549 cells by 19.49% ± 3.13%, 32.41% ± 2.97%, 56.89% ± 5.43%, 72.35% ± 4.39%, and 88.08% ± 4.62% at the doses of 100, 200, 400, 600, and 800 ng/mL, respectively (Figure 11A). Similarly, MTX alone also exhibited substantially elevated caspase-3 activity in A549 cells by 14.49% ± 3.26%, 24.97% ± 4.23%, 42.81% ± 3.99%, 71.30% ± 5.37%, and 91.46% ± 3.44% at the doses of 1, 2, 4, 6, and 8 μg/mL, respectively (Figure 11B). The caspase-8 activity in A549 cells treated with MTX-ZnONPs was substantially augmented by 18.82% ± 1.80%, 29.30% ± 3.67%, 55.81% ± 5.64%, 67.96% ± 2.26%, and 86.33% ± 4.08% at the doses of 100, 200, 400, 600, and 800 ng/mL, respectively (Figure 11A). Likewise, MTX alone also exhibited significantly increased caspase-8 activity in A549 cells by 13.16% ± 2.68%, 22.97% ± 2.46%, 40.81% ± 3.96%, 65.23% ± 4.28%, and 88.66% ± 3.08% at the doses of 1, 2, 4, 6, and 8 μg/mL, respectively

(Figure 11B). Additionally, ZnONPs alone did not exhibit any significant activity of caspase-8 in A549 cells after 24 h of treatment (Figure 11C). Our results demonstrated that, at similar doses, the MTX-ZnONP-treated group showed prominent caspase-9, -8, and -3 activities in A549 cells compared to that treated with MTX alone. Thus, our results established that MTX induced caspase-dependent apoptosis in lung cancer cells via the activation of both intrinsic and extrinsic pathways.

Caspase inhibitors reduced the cytotoxicity

Our results demonstrated that the caspase-3 inhibitor considerably attenuated the cytotoxicity in all the treatment groups, substantiating the activation of caspases in A549 cells

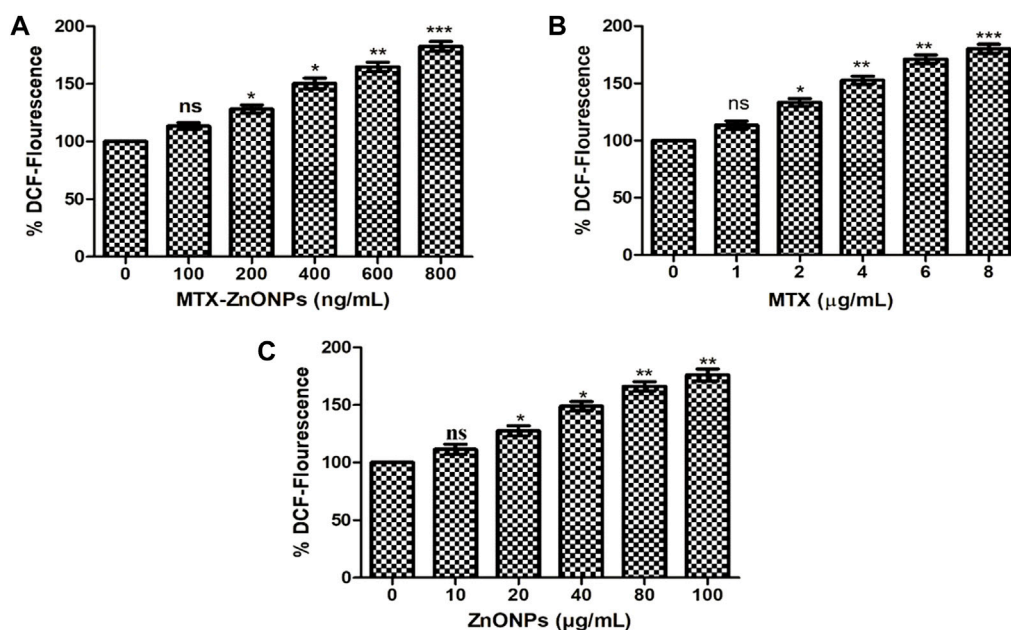


FIGURE 9 Quantitative determination of ROS in H₂DCFDA-stained A549 cells treated with different concentrations of (A) MTX-ZnONPs, (B) MTX alone, and (C) ZnONPs alone for 24 h. The results presented are the mean ± SEM of three independent experiments performed in triplicate. Significance among different dosage groups were determined using one-way ANOVA followed by Dunnett's *post hoc* test (where **p* < 0.05, ***p* < 0.01, and ****p* < 0.001 represent significant differences compared with vehicle control).

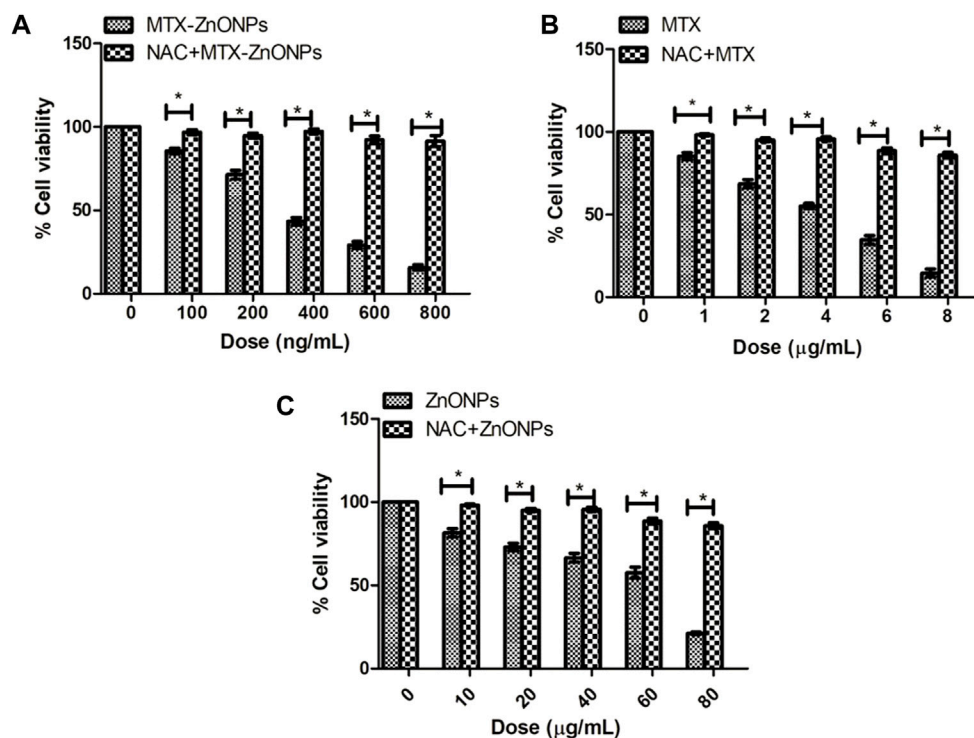


FIGURE 10 Percent cell viability of A549 cells, pretreated with NAC (5 mM), followed by treatment with different doses of (A) MTX-ZnONPs, (B) MTX alone, and (C) ZnONPs alone for 24 h assessed by MTT assay. The results presented are the mean ± SEM of three independent experiments performed in triplicate. Significance among two treatment groups were determined using two-tailed paired *t*-test (where **p* < 0.05 represents significant difference between means of both treatment groups).

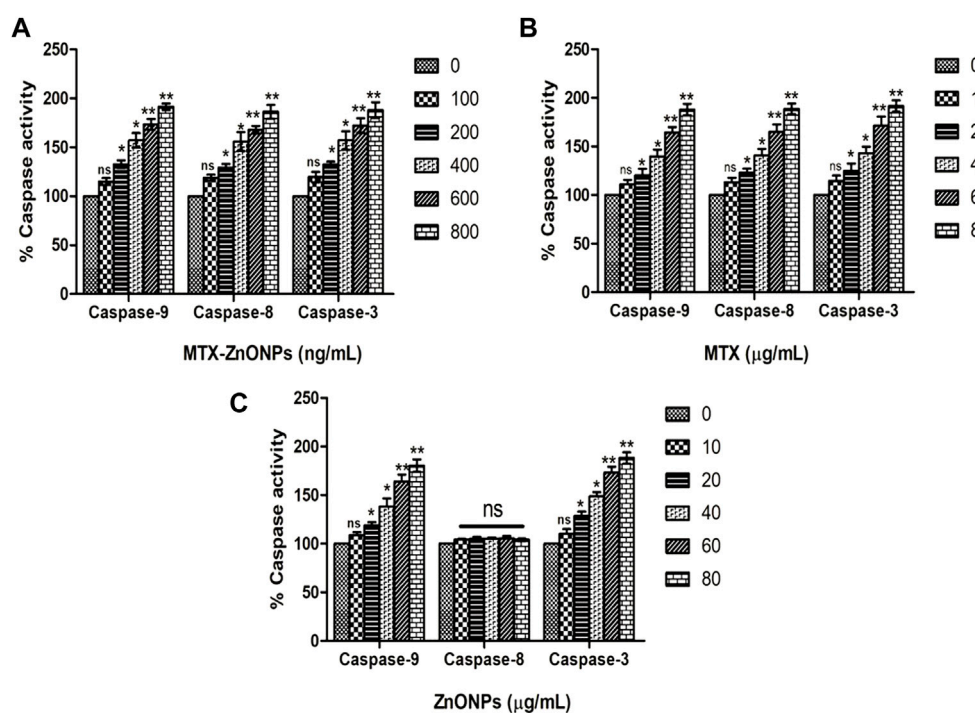


FIGURE 11

Percent caspase-9, -8, and -3 activities in A549 cells treated with different concentrations of (A) MTX-ZnONPs, (B) MTX alone, and (C) ZnONPs alone for 24 h. The results presented are the mean \pm SEM of three independent experiments performed in triplicate. Significance among different dosage groups were determined using one-way ANOVA followed by Dunnett's *post hoc* test (where * $p < 0.05$, ** $p < 0.01$, and *** $p < 0.001$ represent significant differences compared with vehicle control).

(Figure 12). Interestingly, the caspase-3 inhibitor did not completely reduce the cytotoxicity in all the treatment groups, which indicates a minor role of a caspase-independent pathway of apoptosis in A549 cells along with the caspase-dependent pathway.

Discussion

Since standard chemotherapeutic agents often exhibit serious side effects during chemotherapy, their dosage can be reduced by coupling them with some carrier or delivery agent to minimize the side effects of these drugs. This type of conjugation of drugs with some carrier will help deliver drugs directly to the cancer cells. Thus, a lower dose of the drug will be more effective than a higher therapeutic dose (Zhang et al., 2018). In this regard, nanotechnology can offer good drug-delivery options. The biocompatibility and exceptional physicochemical properties of ZnONPs have shown their potential in the diagnosis and treatment of various types of cancer (Hanley et al., 2008; Deng et al., 2009). ZnONPs have been shown to exhibit cytotoxicity in cancer cells by inducing intracellular ROS production and abrogation of $\Delta\Psi_m$, ultimately leading to the activation of caspases and apoptosis (Anjum et al., 2021). For the effective use of ZnONPs, their surface needs to be modified with certain capping (Kalpana et al., 2018; Xu et al., 2018). In this regard, the green synthesis of ZnONPs has received increasing attention recently (Lv et al., 2017). In the current study, biogenically synthesized ZnONPs were conjugated with the antifolate drug

MTX, and their cytotoxic efficacy was determined against lung cancer cells.

We have discussed the biogenic synthesis of ZnONPs using a fungus, later identified as an *A. niger* strain, in the previous publication (Mishra et al., 2017; Mishra et al., 2022). In the current study, we have successfully shown the conjugation of MTX with biogenically synthesized ZnONPs. The conjugation of MTX with ZnONPs was authenticated by UV-vis spectroscopy, DLS, FTIR, and TEM. The drug-nanoconjugate showed high drug-loading efficiency, which indicated the efficiency of ZnONPs as drug carriers. We utilized EDC chemistry to conjugate MTX with ZnONPs. The drug-nanoparticle conjugates were highly stable due to the amide linkage of MTX with ZnONPs.

The cytotoxic efficacy of MTX-ZnONPs was further tested *in vitro* on a non-small cell lung cancer cell line, and the results of MTT and LDH release assays showed that MTX-ZnONPs (at the dose of 100–800 ng/mL) and MTX (at the dose of 1–8 $\mu\text{g/mL}$) were efficient in suppressing the growth of A549 cells; however, the efficacy of MTX-ZnONPs was found to be substantially enhanced at very low doses compared to that of MTX. The most plausible reason behind this enhanced activity of MTX-ZnONPs may be the high drug-loading efficiency of the biogenic nanocarrier and effective delivery of the drug, which could significantly increase the intracellular concentration of MTX, thus enhancing the inhibition of cancer cell proliferation. Interestingly, human folate receptors have been reported to take up MTX-loaded nanoparticles into cells to a better degree than MTX and are most likely to be released only in the acidic environment of lysosomes (Xie et al.,

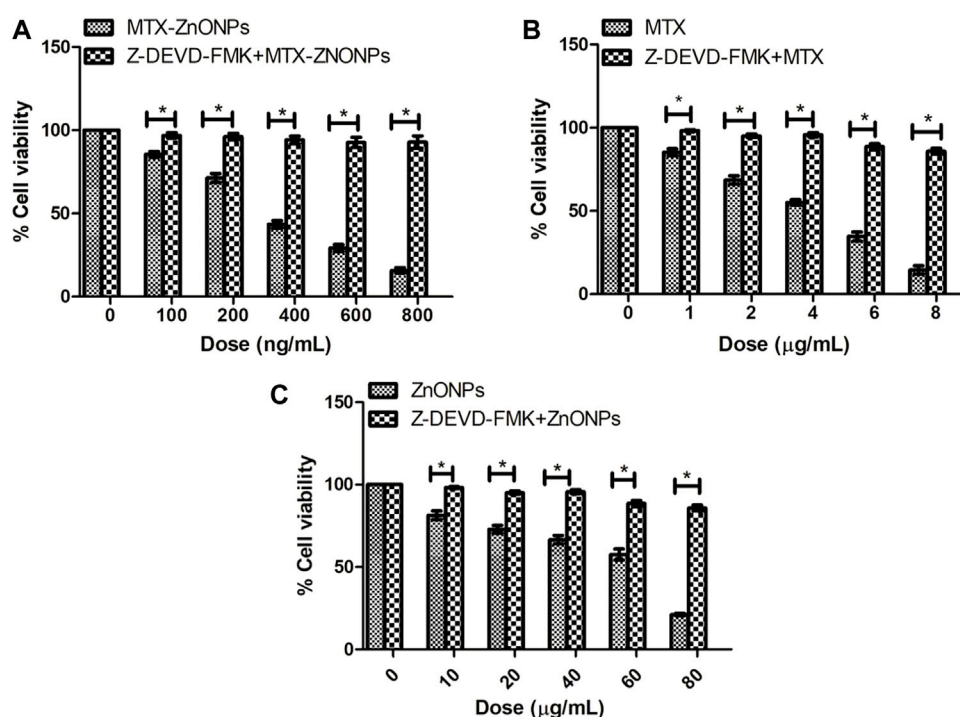


FIGURE 12

Percent cell viability of A549 cells, pretreated with caspase-3 inhibitor Z-DEVD-FMK (50 μ M), followed by treatment with different doses of (A) MTX-ZnONPs, (B) MTX alone, and (C) ZnONPs alone for 24 h assessed by MTT assay. The results presented are the mean \pm SEM of three independent experiments performed in triplicate. Significance among two treatment groups were determined using two-tailed paired *t*-test (where $*p < 0.05$ represents significant difference between means of both treatment groups).

2018). Due to the high expression of the folate receptor on the target cancer cells, MTX-ZnONPs could possibly be internalized inside cancer cells easily and efficiently (Figure 13). Our results were in agreement with a previous study where MTX was conjugated with iron oxide nanoparticles (IONPs) as a drug delivery system to study its cytotoxic effect on cancer cells (Nosrati et al., 2018). Moreover, ZnONPs alone significantly inhibited the cell viability of A549 cells at a much higher concentration (at a dose of 10–80 μ g/mL) compared to MTX-ZnONPs and MTX, which suggested the intrinsic cytotoxic properties of ZnONPs against lung cancer cells at higher concentrations. Previously, the cytotoxic property of ZnONPs was demonstrated in cancer cells, which corroborated our finding (Anjum et al., 2021). Furthermore, our results have also shown a significant cytotoxicity effect of ZnONPs against normal 3T3 cells at a dose range of 10–100 μ g/mL (Supplementary Figure S1). This signified that ZnONPs are cytotoxic not only to A549 cells but also to 3T3 cells at this dose range (Pinho et al., 2020).

When conjugated with MTX, these ZnONPs intriguingly exhibited a similar degree of effect at much lower doses (100–800 ng/mL). This observation might be due to drug alone or the nanocarrier. So, to confirm this observation, we again performed the cell viability assay of A549 cells treated with free ZnONPs at 100–800 ng/mL doses, which showed that ZnONPs were not cytotoxic to A549 cells at the indicated doses (Supplementary Figure S2). This result suggested the non-toxic behavior of free ZnONPs at much lower doses, which could be articulated to be its good nanocarrier property.

Furthermore, cytomorphological analysis performed at isoeffective concentrations by phase contrast microscopy revealed significant changes in the morphology of A549 cells in all the treatment groups, which were evident by cell shrinkage and detachment from the surface, forming clusters. Similarly, the nuclear changes in A549 cells in all the treatment groups, analyzed at isoeffective doses by a fluorescent dye DAPI, revealed fragmented and condensed nuclei, indicating initiation of apoptosis. Interestingly, at isoeffective concentrations, ZnONPs alone exerted similar effects on A549 cells compared to MTX-ZnONPs and MTX alone, which indicated the inherent cytotoxic properties of ZnONPs against lung cancer cells at higher concentrations (Figure 8). Moreover, the results also showed that MTX-ZnONPs exerted similar morphological changes in lung cancer cells at very low doses compared to MTX.

As described previously, the reduction in mitochondrial membrane potential ($\Delta\psi_m$) is an important event during the activation of the intrinsic pathway of apoptosis (Khan I. et al., 2018). Thus, $\Delta\psi_m$ in A549 cells in all the treatment groups, analyzed at isoeffective doses by using a cationic fluorescent dye Rhodamine 123, showed a gradual decrease. ZnONPs alone caused an equivalent reduction in $\Delta\psi_m$ in A549 cells compared to MTX-ZnONPs and MTX alone, which suggested the apoptotic potential of ZnONPs against lung cancer cells at higher doses. Furthermore, the results also showed that MTX-ZnONPs reduced the $\Delta\psi_m$ in lung cancer cells at very low concentrations compared to MTX, suggesting efficient delivery of the drug inside the cell.

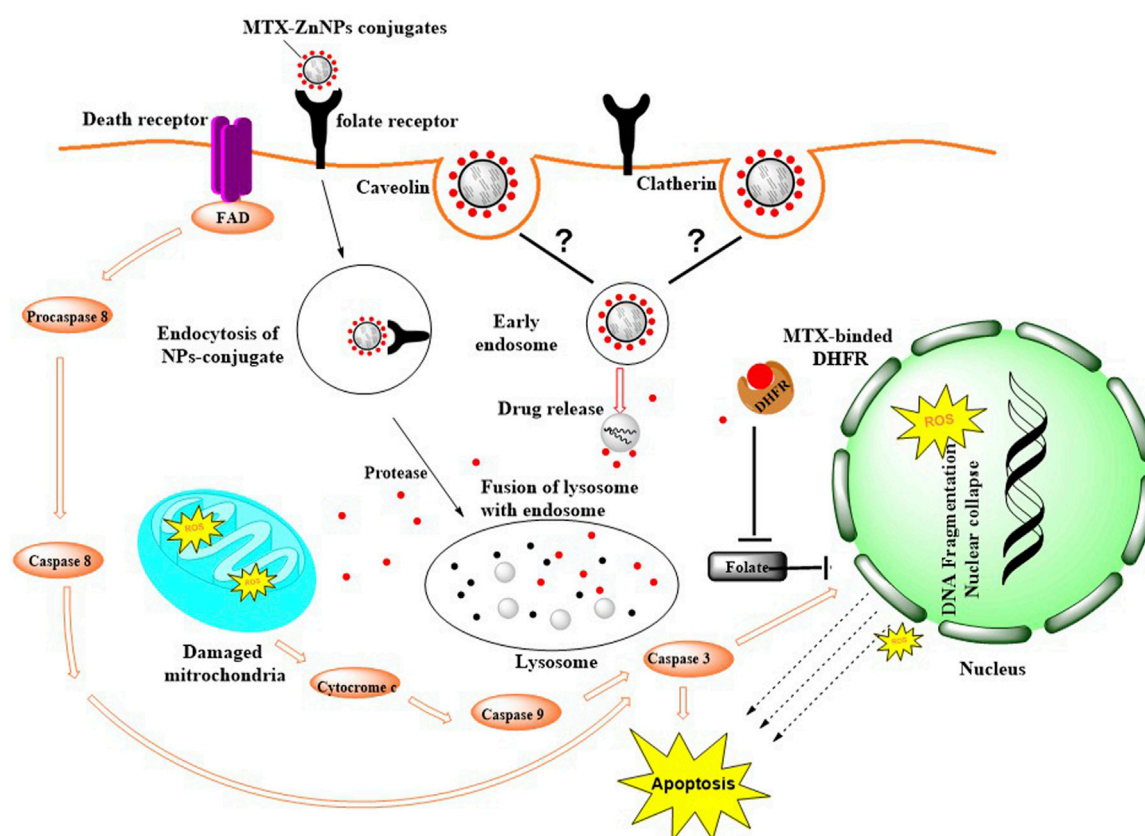


FIGURE 13

Possible mode of internalization of MTX-ZnONPs via caveolin-mediated or clathrin-mediated endocytosis and mechanism of action of MTX in A549 cells.

Many anticancer drugs exert their therapeutic effect on cancer cells by augmenting the production of cytosolic ROS (Doroshov, 1986; Oh et al., 2007). ROS have been implicated in many cellular functions, such as apoptosis (Nakazato et al., 2007). Results of qualitative analysis of ROS, analyzed at isoeffective doses in A549 cells in all the treatment groups, depicted an augmented intracellular ROS level. Intriguingly, ZnONPs alone induced a similar amount of ROS generation in A549 cells compared to MTX-ZnONPs and MTX at isoeffective doses, which suggested that ZnONPs alone caused ROS-dependent apoptosis in lung cancer cells at higher doses. Furthermore, the results also showed that MTX-ZnONPs induced a similar amount of ROS in lung cancer cells at very low concentrations compared to MTX. Thus, our results suggested that MTX primarily caused ROS-mediated cell death in A549 cells.

Additionally, the results of quantitative analysis of ROS revealed that MTX-ZnONPs (at the dose of 100–800 ng/mL) and MTX alone (at the dose of 1–8 µg/mL) were effective in augmenting the intracellular ROS level in A549 cells; however, the effect of MTX-ZnONPs was more profound at very low doses compared to that of MTX. Moreover, ZnONPs alone substantially elevated the ROS level in A549 cells at much higher concentrations (10–80 µg/mL) compared to MTX-ZnONPs and MTX alone, which illustrated that the cytotoxic property of ZnONPs was due to ROS-mediated programmed cell death in lung cancer cells at higher concentrations.

To corroborate the production of ROS in all the treatment groups, cell survival was estimated in lung cancer cells pretreated with NAC. It was observed that NAC significantly ameliorated the cell viability in all the treatment groups, authenticating the crucial role of ROS-mediated apoptosis in A549 cells. Interestingly, NAC did not completely ameliorate the survival of A549 cells in all the treatment groups, which indicated the role of ROS-independent pathways of apoptosis in A549 cells. Thus, our results showed that MTX could induce apoptosis in lung cancer cells via both ROS-dependent and ROS-independent pathways.

It has been well established that caspase-8 and caspase-9 play indispensable roles in the activation of the extrinsic and intrinsic apoptotic pathways, respectively (Ona et al., 1999). Moreover, caspase-3 is the chief executor of apoptosis by cleaving and dismantling the cellular structures (Bakar et al., 2010). Therefore, to confirm whether the cell death induced in lung cancer cells in all the treatment groups was due to the extrinsic or intrinsic pathway of apoptosis, caspase activities were determined in A549 cells. The results showed that MTX-ZnONPs (at the dose of 100–800 ng/mL) and MTX alone (at the dose of 1–8 µg/mL) caused significant activation of caspase-9, -8, and -3 in A549 cells; however, the effect of MTX-ZnONPs was more profound at very low doses compared to that of MTX. These results suggested that MTX induced apoptosis in A549 cells via both extrinsic and intrinsic pathways. Moreover, ZnONPs alone substantially activated caspase-

9 and -3 in A549 cells at much higher concentrations (10–80 µg/mL) compared to MTX-ZnONPs (at the dose of 100–800 ng/mL) and MTX alone (at the dose of 1–8 µg/mL), while there was no significant activation of caspase-8, illustrating the activation of only the mitochondrial pathway of programmed cell death in lung cancer cells treated with ZnONPs at higher concentrations.

To validate the activation of caspases in lung cancer cells, cell survival was estimated in all the treatment groups pretreated with the caspase-3 inhibitor. The results showed that pre-treatment with the caspase-3 inhibitor significantly ameliorated the cell viability, demonstrating the instigation of caspases during programmed cell death in A549 cells in all the treatment groups. Intriguingly, pretreatment with a caspase-3 inhibitor did not completely ameliorate cell viability in lung cancer cells, indicating the activation of a caspase-independent pathway of apoptosis in A549 cells. Thus, our results showed that MTX could induce apoptosis in lung cancer cells via both caspase-dependent and caspase-independent pathways.

Conclusion

In conclusion, the results of the current study have illustrated the conjugation of MTX with ZnONPs with high drug-loading efficiency. Moreover, the cytotoxic efficiency of MTX-ZnONPs was found to be enhanced compared to MTX alone in lung cancer cells. ZnONPs exhibited significant toxicity against lung cancer cells only at very high doses compared to the effective doses of drug-nanoconjugates, which suggested that the high therapeutic efficiency of MTX-ZnONPs was due to intracellular delivery of MTX. Thus, our results emphasized the efficient delivery of MTX to lung cancer cells via ZnONPs as nanocarriers.

Data availability statement

The original contributions presented in the study are included in the article/[Supplementary Material](#); further inquiries can be directed to the corresponding authors.

Author contributions

Conceptualization: IA and PM; methodology: PM and MFA; software: IA, MS, and NA; validation: MS, PM, MFA, MV, SF, AA, and NA; formal analysis: LK, NMA, MS, and NA; investigation: PM and AA; resources: MS, NMA, LK, and IA; data curation: IA; writing—original draft preparation: PM; writing—review and

editing: IA; visualization: IA, MS, and LK; supervision: IA and LK; project administration: IA, MS, and LK.

Acknowledgments

The authors are thankful to the Princess Nourah bint Abdulrahman University researcher supporting program number (PNURSP2023R82), Princess Nourah bint Abdulrahman University, Riyadh, Saudi Arabia.

Conflict of interest

The authors declare that the research was conducted in the absence of any commercial or financial relationships that could be construed as a potential conflict of interest.

Publisher's note

All claims expressed in this article are solely those of the authors and do not necessarily represent those of their affiliated organizations, or those of the publisher, the editors, and the reviewers. Any product that may be evaluated in this article, or claim that may be made by its manufacturer, is not guaranteed or endorsed by the publisher.

Supplementary material

The Supplementary Material for this article can be found online at: <https://www.frontiersin.org/articles/10.3389/fphar.2023.1194578/full#supplementary-material>

SUPPLEMENTARY FIGURE S1

Percent cell viability of 3T3 cells treated with different doses of ZnONPs for 24 h assessed by MTT assay. The results presented are the mean ± SEM of three independent experiments performed in triplicate. Significance among different dosage groups were determined using one-way ANOVA followed by Dunnett's *post hoc* test (where **p* < 0.05, ***p* < 0.01, and ****p* < 0.001 represent significant differences compared with vehicle control).

SUPPLEMENTARY FIGURE S2

Percent cell viability of A549 cells in all the treatment groups treated with the effective doses of MTX-ZnONPs (100–800 ng/mL) for 24 h. The results presented are the mean ± SEM of three independent experiments performed in triplicate. Significance in different treatment groups at different doses were determined using two-way ANOVA with Bonferroni's *post hoc* tests (where **p* < 0.05, ***p* < 0.01, and ****p* < 0.001 represent significant differences between means of different treatment groups at different doses).

References

- Aghajanzadeh, M., Zamani, M., Molavi, H., Khieri Manjili, H., Danafar, H., and Shojaei, A. (2018). Preparation of metal–organic frameworks UiO-66 for adsorptive removal of methotrexate from aqueous solution. *J. Inorg. Organomet. Polym. Mater.* 28 (1), 177–186. doi:10.1007/s10904-017-0709-3
- Anjum, S., Hashim, M., Malik, S. A., Khan, M., Lorenzo, J. M., Abbasi, B. H., et al. (2021). Recent advances in zinc oxide nanoparticles (ZnO NPs) for cancer diagnosis, target drug delivery, and treatment. *Cancers* 13 (18), 4570. doi:10.3390/cancers13184570
- Bakar, M. F. A., Mohamad, M., Rahmat, A., Burr, S. A., and Fry, J. R. (2010). Cytotoxicity, cell cycle arrest, and apoptosis in breast cancer cell lines exposed to an extract of the seed kernel of *Mangifera pajang* (bambangan). *Food Chem. Toxicol.* 48 (6), 1688–1697. doi:10.1016/j.ft.2010.03.046
- Barui, A. K., Kotcherlakota, R., and Patra, C. R. (2018). "Biomedical applications of zinc oxide nanoparticles," in *Inorganic frameworks as smart nanomedicines* (Amsterdam, Netherlands: Elsevier), 239–278.

- Crews, K. R., Liu, T., Rodriguez-Galindo, C., Tan, M., Meyer, W. H., Panetta, J. C., et al. (2004). High-dose methotrexate pharmacokinetics and outcome of children and young adults with osteosarcoma. *Cancer Interdiscip. Int. J. Am. Cancer Soc.* 100 (8), 1724–1733. doi:10.1002/cncr.20152
- Deng, X., Luan, Q., Chen, W., Wang, Y., Wu, M., Zhang, H., et al. (2009). Nanosized zinc oxide particles induce neural stem cell apoptosis. *Nanotechnology* 20 (11), 115101. doi:10.1088/0957-4484/20/11/115101
- Doroshov, J. H. (1986). Role of hydrogen peroxide and hydroxyl radical formation in the killing of Ehrlich tumor cells by anticancer quinones. *Proc. Natl. Acad. Sci.* 83 (12), 4514–4518. doi:10.1073/pnas.83.12.4514
- Duncan, R., and Richardson, S. C. W. (2012). Endocytosis and intracellular trafficking as gateways for nanomedicine delivery: opportunities and challenges. *Mol. Pharm.* 9 (9), 2380–2402. doi:10.1021/mp300293n
- Duthie, S. J. (2001). Folic-acid-mediated inhibition of human colon-cancer cell growth. *Nutrition* 17 (9), 736–737. doi:10.1016/s0899-9007(01)00595-0
- Evans, W. E., Crom, W. R., Abromowitch, M., Dodge, R., Look, A. T., Bowman, W. P., et al. (1986). Clinical pharmacodynamics of high-dose methotrexate in acute lymphocytic leukemia. Identification of a relation between concentration and effect. *N. Engl. J. Med.* 314 (8), 471–477. doi:10.1056/NEJM198602203140803
- Frei, E., III, Jaffe, N., Tattersall, M. H. N., Pitman, S., and Parker, L. (1975). New approaches to cancer chemotherapy with methotrexate. *N. Engl. J. Med.* 292 (16), 846–851. doi:10.1056/NEJM197504172921607
- Gewirtz, D. A., Bristol, M. L., and Yalowich, J. C. (2010). Toxicity issues in cancer drug development. *Curr. Opin. investigational drugs (London, Engl. 2000)* 11 (6), 612–614.
- Gomathy, M., and Sabarinathan, K. G. (2010). Microbial mechanisms of heavy metal tolerance—a review. *Agric. Rev.* 31 (2).
- Hanley, C., Layne, J., Punnoose, A., Reddy, K., Coombs, I., Coombs, A., et al. (2008). Preferential killing of cancer cells and activated human T cells using ZnO nanoparticles. *Nanotechnology* 19 (29), 295103. doi:10.1088/0957-4484/19/29/295103
- Huenekens, F. M. (1994). The methotrexate story: A paradigm for development of cancer chemotherapeutic agents. *Adv. enzyme Regul.* 34, 397–419. doi:10.1016/0065-2571(94)90025-6
- Kalpana, V. N., Kataru, B. A. S., Sravani, N., Vigneshwari, T., Panneerselvam, A., and Rajeswari, V. D. (2018). Biosynthesis of zinc oxide nanoparticles using culture filtrates of *Aspergillus Niger*: antimicrobial textiles and dye degradation studies. *OpenNano* 3, 48–55. doi:10.1016/j.onano.2018.06.001
- Khan, I., Khan, F., Farooqui, A., and Ansari, I. A. (2018a). Andrographolide exhibits anticancer potential against human colon cancer cells by inducing cell cycle arrest and programmed cell death via augmentation of intracellular reactive oxygen species level. *Nutr. cancer* 70 (5), 787–803. doi:10.1080/01635581.2018.1470649
- Khan, S., Ahmad, K., Ahmad, A., Raish, M., Jan, B. L., Khan, A., et al. (2018b). Biogenic pentagonal silver nanoparticles for safer and more effective antibacterial therapeutics. *Int. J. nanomedicine* 13, 7789–7799. doi:10.2147/IJN.S168224
- Khan, Z. A., Tripathi, R., and Mishra, B. (2012). Methotrexate: A detailed review on drug delivery and clinical aspects. *Expert Opin. drug Deliv.* 9 (2), 151–169. doi:10.1517/17425247.2012.642362
- Lee, S. H. (2019). Chemotherapy for lung cancer in the era of personalized medicine. *Tuberc. Respir. Dis.* 82 (3), 179–189. doi:10.4046/trd.2018.0068
- Lv, Y., Liu, R., Xie, S., Zheng, X., Mao, J., Cai, Y., et al. (2017). Calcein-acetoxymethyl ester enhances the antitumor effects of doxorubicin in nonsmall cell lung cancer by regulating the TopBP1/p53RR pathway. *Anti-cancer drugs* 28 (8), 861–868. doi:10.1097/CAD.0000000000000527
- Mishra, P., Ahmad, A., Al-Keridis, L. A., Alshammari, N., Alabdallah, N. M., Muzammil, K., et al. (2022). Doxorubicin-conjugated zinc oxide nanoparticles, biogenically synthesised using a fungus *Aspergillus Niger*, exhibit high therapeutic efficacy against lung cancer cells. *Molecules* 27 (8), 2590. doi:10.3390/molecules27082590
- Mishra, P. K., Mishra, H., Ekielski, A., Talegaonkar, S., and Vaidya, B. (2017). Zinc oxide nanoparticles: A promising nanomaterial for biomedical applications. *Drug Discov. today* 22 (12), 1825–1834. doi:10.1016/j.drudis.2017.08.006
- Nakazato, T., Sagawa, M., Yamato, K., Xian, M., Yamamoto, T., Suematsu, M., et al. (2007). Myeloperoxidase is a key regulator of oxidative stress-mediated apoptosis in myeloid leukemic cells. *Clin. Cancer Res.* 13 (18), 5436–5445. doi:10.1158/1078-0432.CCR-07-0481
- Nosrati, H., Salehiabar, M., Davaran, S., Danafar, H., and Manjili, H. K. (2018). Methotrexate-conjugated L-lysine coated iron oxide magnetic nanoparticles for inhibition of MCF-7 breast cancer cells. *Drug Dev. industrial Pharm.* 44 (6), 886–894. doi:10.1080/03639045.2017.1417422
- Nosrati, H., Salehiabar, M., Davaran, S., Ramazani, A., Manjili, H. K., and Danafar, H. (2017). New advances strategies for surface functionalization of iron oxide magnetic nano particles (IONPs). *Res. Chem. Intermed.* 43 (12), 7423–7442. doi:10.1007/s11164-017-3084-3
- Nunez, M. I., Behrens, C., Woods, D. M., Lin, H., Suraokar, M., Kadara, H., et al. (2012). High expression of folate receptor alpha in lung cancer correlates with adenocarcinoma histology and EGFR [corrected] mutation. *J. Thorac. Oncol.* 7 (5), 833–840. doi:10.1097/JTO.0b013e31824de09c
- Oh, S. Y., Sohn, Y. W., Park, J. W., Park, H. J., Jeon, H. M., Kim, T. K., et al. (2007). Selective cell death of oncogenic Akt-transduced brain cancer cells by etoposide through reactive oxygen species-mediated damage. *Mol. cancer Ther.* 6 (8), 2178–2187. doi:10.1158/1535-7163.MCT-07-0111
- Ona, V. O., Li, M., Vonsattel, J. P. G., Andrews, L. J., Khan, S. Q., Chung, W. M., et al. (1999). Inhibition of caspase-1 slows disease progression in a mouse model of Huntington's disease. *Nature* 399 (6733), 263–267. doi:10.1038/20446
- O'Shannessy, D. J., Yu, G., Smale, R., Fu, Y. S., Singhal, S., Thiel, R. P., et al. (2012). Folate receptor alpha expression in lung cancer: diagnostic and prognostic significance. *Oncotarget* 3 (4), 414–425. doi:10.18632/oncotarget.489
- Pinho, A. R., Martins, F., Costa, M. E. V., Senos, A. M. R., da Cruz e Silva, O. A. B., Pereira, M. de L., et al. (2020). *In vitro* cytotoxicity effects of zinc oxide nanoparticles on spermatogonia cells. *Cells* 9 (5), 1081. doi:10.3390/cells9051081
- Singh, T. A., Das, J., and Sil, P. C. (2020). Zinc oxide nanoparticles: A comprehensive review on its synthesis, anticancer and drug delivery applications as well as health risks. *Adv. colloid interface Sci.* 286, 102317. doi:10.1016/j.cis.2020.102317
- Xie, J., Fan, Z., Li, Y., Zhang, Y., Yu, F., Su, G., et al. (2018). Design of pH-sensitive methotrexate prodrug-targeted curcumin nanoparticles for efficient dual-drug delivery and combination cancer therapy. *Int. J. nanomedicine* 13, 1381–1398. doi:10.2147/IJN.S152312
- Xu, S., Sun, T., Xu, Q., Duan, C., Dai, Y., Wang, L., et al. (2018). Preparation and antibiofilm properties of zinc oxide/porous anodic alumina composite films. *Nanoscale Res. Lett.* 13 (1), 201–212. doi:10.1186/s11671-018-2568-4
- Zamani, M., Rostami, M., Aghajanzadeh, M., Kheiri Manjili, H., Rostamizadeh, K., and Danafar, H. (2018). Mesoporous titanium dioxide@ zinc oxide-graphene oxide nanocarriers for colon-specific drug delivery. *J. Mater. Sci.* 53 (3), 1634–1645. doi:10.1007/s10853-017-1673-6
- Zhang, T., Chen, Y., Ge, Y., Hu, Y., Li, M., and Jin, Y. (2018). Inhalation treatment of primary lung cancer using liposomal curcumin dry powder inhalers. *Acta Pharm. Sin.* B 8 (3), 440–448. doi:10.1016/j.apsb.2018.03.004